Sea-ice concentration retrieval in the Antarctic based on the SSM/I 85.5 GHz polarization

Stefan Kern,[*] Georg Heygster

Institute of Environmental Physics, P.O. Box 330440, D-28334 Bremen, Germany

ABSTRACT. Using data from the 85 GHz channels of the Special Sensor Microwave/ Imager (SSM/I) allows a resolution improvement by at least a factor of four compared to the other channels. Consequently, higher-resolution sea-ice concentration data can be obtained which in turn can be used to improve the results of numerical weather-prediction (NWP) and global circulation models. The proposed new sea-ice concentration retrieval algorithm (SEA LION algorithm) uses the polarization at 85 GHz (P). Emission from atmospheric water and scattering at the wind-roughened sea surface (weather effect) decrease P and cause an overestimation of the sea-ice concentration. We quantify the weather effect with a radiative transfer model and atmospheric data obtained from NWP models and the other SSM/I channels, and correct P for this effect. Tie points of open water and sea ice are determined for each month separately from daily gridded 85 GHz SSM/I brightness temperatures. Sea-ice concentrations are calculated with the new algorithm for the entire Southern Ocean for each day of the period 1992–98 with a spatial resolution of 12.5×12.5 km^2. Comparisons of these ice concentrations with Operational Linescan System visible images reveal convincing results concerning the monitoring of coastal polynyas and the break-up of the pack ice in spring. SEA LION sea-ice extents and areas, and comparisons between SEA LION sea-ice concentrations and ship observations, agree with those obtained by the NASA Team and the Bootstrap algorithms.

1. INTRODUCTION

In this paper, we describe and test a new algorithm, which exploits the higher spatial resolution of the 85 GHz channels of the Special Sensor Microwave/Imager (SSM/I) to retrieve higher-resolution daily sea-ice concentration data than are currently provided by other algorithms. The SSM/I sensor, first launched in 1987 as part of the Defense Meteorological Satellite Program (DMSP), scans the Earth's surface conically with a constant ground-surface incidence angle of 53.1° and is equipped with channels operating at 19.35, 37.0 and 85.5 GHz with both vertical and horizontal polarization, and at 22.235 GHz with vertical polarization alone (Hollinger and others, 1987). Among others, the Bootstrap (Comiso and others, 1992) and the NASA Team (Cavalieri and others, 1991) algorithms, which are based on the 19 and 37 GHz channels, are generally used for routine sea-ice concentration retrieval. However, both algorithms suffer from the sensor's large footprint of 69×43 km^2 (at 19 GHz) and of 37×28 km^2 (37 GHz). The footprint at 85 GHz (15×13 km^2) allows a much better spatial resolution. Svendsen and others (1987) were the first to use frequencies near 90 GHz for sea-ice concentration retrieval. Their results are based on the brightness-temperature polarization difference (BTPD) and have been

validated for clear-sky winter (Lomax and others, 1995) and overcast summer conditions (Lubin and others, 1997).

We use the *normalized* BTPD (NBTPD) (also called polarization) at 85 GHz instead of the BTPD to minimize the influence of changing physical temperatures of the radiating portion of the sea ice. The other SSM/I channels are not used to retrieve the sea-ice concentration in this study.

Sea ice significantly reduces the exchange of sensible and latent heat as well as momentum between the polar ocean and atmosphere (Maykut, 1978). Gaining an accurate knowledge of the associated surface fluxes is very important for modeling atmospheric dynamics and thermodynamics with numerical weather-prediction (NWP) models. Over sea ice, the quality of the modeled fluxes is largely determined by the sea-ice concentration, which can be calculated from space-borne remote-sensing data, as well as its thickness and roughness, quantities that are more difficult to estimate from these data. The spatial resolution of space-borne remote-sensing data covers several orders of magnitude, from ~25 m for the synthetic aperture radar (SAR) to > 25 km for the SSM/I. Though SAR is an excellent source for detailed information on type and structure of a sea-ice cover (Drinkwater, 1998), larger- (hemispherical-)scale geophysical parameters, such as sea-ice concentration obtained from SSM/I data, are more convenient for use in NWP and global circulation models.

The following sections will focus on the new algorithm and possible error sources. The effects of snow cover and intervening atmosphere, which vary both spatially and temporally,

---

[*] Present address: Insitute of Oceanography, Troplowitzstrasse 7, D-22529 Hamburg, Germany.

Table 1. *Surface emissivities ε_v and ε_h and their standard deviations σ_v and σ_h measured in situ at 90 GHz in the Weddell Sea, Antarctica (Comiso and others, 1992), and the NBTPD P and corresponding standard deviations (P) as calculated from these measurements*

90 GHz	Open water	Gray nilas	White nilas
$\varepsilon_v \pm \sigma_v$	0.785 ± 0.050	0.922 ± 0.020	0.961 ± 0.024
$\varepsilon_h \pm \sigma_h$	0.530 ± 0.060	0.841 ± 0.051	0.927 ± 0.018
$P \pm \sigma_P$	0.194 ± 0.024	0.046 ± 0.019	0.018 ± 0.003

90 GHz	Pancake ice	Cold FY ice	Melting FY ice
$\varepsilon_v \pm \sigma_v$	0.941 ± 0.058	0.954 ± 0.036	0.921 ± 0.039
$\varepsilon_h \pm \sigma_h$	0.892 ± 0.063	0.919 ± 0.026	0.881 ± 0.027
$P \pm \sigma_P$	0.027 ± 0.004	0.019 ± 0.005	0.022 ± 0.006

are discussed and accounted for by the use of temporal tie points and a radiative transfer model, respectively. The new algorithm is used to calculate daily sea-ice concentration data for the period 1992–98. Examples are compared with independent data for validation purposes.

2. METHODS

The basis of the algorithm presented, henceforth referred to as SEA LION, is as follows. The brightness temperature T_p, emitted at polarization p from a partly sea-ice-covered ocean area equal to unity, with the fractions of sea ice C and open water $(1 - C)$, can be written as:

$$T_p = (1 - C)\varepsilon_{pw}T_{sw} + C\varepsilon_{pi}T_{si} , \qquad (1)$$

where the emissivities of open water and sea ice at polarization p are given by ε_{pw} and ε_{pi}, respectively, and T_{sw} and T_{si} are the physical temperatures of the sea surface and of the radiating sea-ice portion, respectively. This approach follows that of Svendsen and others (1987) but omits multi-year ice since Antarctic sea ice primarily consists of first-year (FY) ice. The NBTPD, which is also used in the NASA Team algorithm, is defined as:

$$P = (T_v - T_h)(T_v + T_h)^{-1} , \qquad (2)$$

where T_v and T_h are the brightness temperatures at vertical and horizontal polarization, respectively. The NBTPD calculated from emissivities, which have been measured in situ at 90 GHz in the Weddell Sea (Comiso and others, 1992), is small over sea ice but quite large over open water (Table 1). Inserting Equation (1) into Equation (2) yields:

$$C = [1 + a(P_i - P)(P - P_w)^{-1}]^{-1} , \qquad (3)$$

where a is given by

$$a = (T_{vi} + T_{hi})(T_{vw} + T_{hw})^{-1} . \qquad (4)$$

The triplets P_w, T_{vw}, T_{hw} and P_i, T_{vi}, T_{hi} are the tie points of open water and sea ice, respectively (section 2.1), which we calculate prior to the retrieval of C (section 2.3). Since Equation (3) is valid for surface measurements only, the use of SSM/I data requires a consideration of the atmospheric effect (section 2.2).

2.1. Tie points

The wavelength at 85 GHz is small compared to the other SSM/I channels. This has two consequences. One is that sea ice becomes radiometrically opaque at a smaller thickness (Grenfell and others, 1998). Secondly, emission and, more important, scattering in the snow provide a significant contribution to the radiometric signal of snow-covered sea ice (Grenfell and others, 1994, 1998) and may smooth different signals associated with different sea-ice types. However, the snow-cover properties (e.g. the liquid-water content, the grain-size and the density) exhibit a large spatial and temporal variability, and can change on daily to seasonal time-scales due to snow metamorphism and precipitation (Garrity, 1992; Massom and others, 1998; Sturm and others, 1998).

Taking this into account, the emissivities, which are given in Table 1 and which have been measured in the Weddell Sea in winter and spring only (Comiso and others, 1992), are not representative for the sea-ice conditions of the entire Antarctic all the year round. Considering this lack of information and the highly varying snow properties, we decided to derive sea-ice tie points for each month separately as follows. Monthly averages of the NBTPD, P_{AVE}, and the temporal variability (variance), σ_P^2, are calculated for each pixel using the U.S. National Snow and Ice Data Center (NSIDC) daily gridded SSM/I brightness temperatures. The averages of P (not shown) allow the separation of sea ice ($P_{AVE} < 0.05$) from open water ($P_{AVE} > 0.12$). However, over open water, P_{AVE} is significantly smaller than P obtained from in situ measurements of ε_v and ε_h (Table 1), due to the monthly-averaged weather effect, which extends also into the sea-ice zone. The variances of P (not shown) increase towards the marginal ice zone (MIZ), i.e. pixels that are closer to the MIZ exhibit a larger temporal variability than pixels from the inner pack. This can be explained by an increasing variability of C and an increase of the direct (atmospheric water content) and indirect (precipitation, melt–freeze cycles, flooding) weather influences towards the MIZ. Over polynyas, P_{AVE} is smaller and σ_P^2 is larger than in other pack-ice areas, since C and atmospheric water contents are more variable.

The sea-ice tie points T_{vi}, T_{hi} and P_i are calculated by averaging only values of T_v, T_h and P from areas where $P_{AVE} < 0.05$ and $\sigma_P^2 < 25 \times 10^{-6}$ ($\sigma_P < 0.005$; Table 1) for the given month. Thus, almost all pixels with $C < 100\%$ and with a highly variable polarization, due to either changing surface properties or weather conditions or both, are excluded. The high limit chosen for P_{AVE} ensures that nilas (Table 1) is considered.

Open-water tie points T_{vw}, T_{hw} and P_w are also calculated for each month separately from NSIDC daily gridded SSM/I brightness temperatures within clear-sky areas, which have been extracted from daily maps of the integrated cloud liquid-water content L ($L \leq 15 \text{ g m}^{-2}$ = clear sky) (Karstens and others, 1994; Heygster and others, 1996) and which simultaneously exhibit a surface wind speed $V < 10 \text{ m s}^{-1}$ and an integrated water-vapour content $W < 10 \text{ kg m}^{-2}$. Finally, the remaining direct weather effects on the tie points over open water of V and W, and over sea ice of W only, are quantified and subtracted (section 2.2).

2.2. Atmospheric effects

Compared to the Arctic, the atmospheric effect on SSM/I measurements is much more pronounced in the Antarctic sea-ice zone due to its proximity to the Southern Ocean, which is a substantial source of atmospheric heat and moisture and a site of significant cyclogenesis (King and Turner,
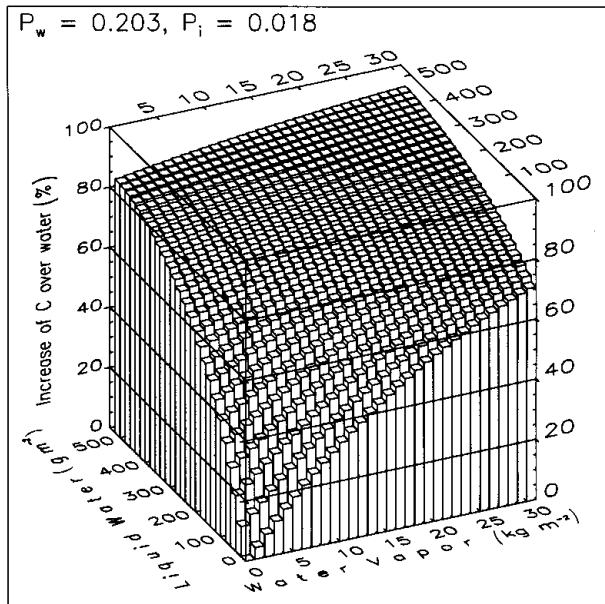
110

Fig. 1. Increase of C due to W and L as calculated with Equation (3) from uncorrected 85 GHz SSM/I brightness temperatures over a calm sea surface with C = 0% and the tie points of sea ice and open water as given in the upper left corner.

1997). The increase of the SSM/I brightness temperatures due to emission from atmospheric water, which mainly consists of W and L, is larger at 85 GHz than at the other SSM/I channels (Ulaby and others, 1981). Though this increase is less significant over most sea-ice-covered areas due to their high surface emissivities, it becomes larger with decreasing surface emissivities (e.g. over the MIZ: Fuhrhop and others, 1998). Figure 1 shows the increase of C due to W and L as calculated from uncorrected 85 GHz SSM/I brightness temperatures with Equation (3) for a calm sea surface (salinity: 34 ppt; surface temperature: 0°C; $C = 0\%$). Over open water, C could increase to 90% or more. Over 100% of cold FY ice (Table 1), this increase (not shown) is still one-tenth of that over open water.

In order to quantify the effect of W and L, we have modeled brightness temperatures with the radiative transfer model MWMOD (MicroWave MODel) (Fuhrhop and others, 1998) for emissivities of 0.44–0.98 in increments of 0.01 and typical values of W and L. For each emissivity, a two-dimensional polynomial fit yields a set of coefficients that allows the subtraction of the quantified atmospheric water effect from the SSM/I brightness temperatures if W, L and the emissivities are known. While W is taken from the operational NWP model of the European Centre for Medium-range Weather Forecasts (ECMWF) over both open ocean and sea ice, this is not possible for L. Over open water, L has been calculated with the method given by Karstens and others (1994), a method which cannot be applied over sea ice. Miao and others (2000) developed what they call the R-factor method to identify regions where $L \geq 100\,\mathrm{g\,m^{-2}}$. We used this method to successfully mask out about 75% of such regions over open water and sea ice. The remaining 25% with $L \geq 100\,\mathrm{g\,m^{-2}}$ account for < 5% of the total area covered by the NSIDC grid used. Now we use daily sea-ice concentration maps, which are based on the NASA Team algorithm, as a mask to predefine water- and ice-covered areas. Over sea ice, we set L to its monthly-average value obtained from daily

data of L within an approximately 100 km wide open-water area adjacent to the sea-ice edge. These averages vary between 40 and 80 $\mathrm{g\,m^{-2}}$ in winter and summer, respectively. This was done considering the high percentage of clouds covering the Southern Ocean (70% according to the results of the International Satellite Cloud Climatology Project (ISCCP)), and the lack of reliable data of L.

Over sea ice, the ratios of $T_{vi} - \mathrm{d}T_{vi}(O_2)$ or $T_{hi} - \mathrm{d}T_{hi}(O_2)$ and the monthly-averaged ECMWF surface temperatures are taken as the emissivity. The quantities $\mathrm{d}T_{vi}(O_2)$ and $\mathrm{d}T_{hi}(O_2)$ denote brightness-temperatures contributions due to oxygen absorption as quantified with MWMOD. Over open water, the emissivities are altered by the surface wind (Ulaby and others, 1981). In particular, $V > 10\,\mathrm{m\,s^{-1}}$ significantly decrease P at 85 GHz, again causing an overestimation of C if neglected. We used MWMOD to calculate sea-surface emissivities and to model the change of T_v and T_h for typical wind speeds, which have also been taken from the ECMWF model. The emissivities are put into a look-up table. For a given V, this table provides the correct sea-surface emissivity required by the correction for the effect of W and L on T_v and T_h. The changes of T_v and T_h according to V are subtracted from the brightness temperatures after this correction by using a set of coefficients, obtained with a one-dimensional polynomial fit from the modeled brightness temperatures.

2.3. Algorithm

Equation (3) is the basis of the SEA LION algorithm, which iteratively calculates and minimizes the difference between P obtained from the uncorrected NSIDC daily gridded 85 GHz SSM/I brightness temperatures and P obtained from brightness temperatures that have been modeled for the given atmospheric conditions and the retrieved C. The first iteration step is to calculate a first-guess sea-ice concentration C_{FG} using Equation (3) and uncorrected SSM/I data in all regions which have not been masked out using the R-factor method. In order to prove C_{FG}, brightness temperatures are modeled with MWMOD according to the values of W, L, V and C_{FG}. If P obtained from these modeled brightness temperatures differs from the measured one by < 0.001, which is about 1% change in C, then C_{FG} is taken as the actual sea-ice concentration, and the iteration is stopped. Otherwise the weather effect given by W, L and V is quantified and subtracted from the SSM/I brightness temperatures. A first-order weather-corrected P is calculated from these corrected SSM/I brightness temperatures and is used to calculate a *new* first-guess sea-ice concentration, similar to the first iteration step. The *new* C_{FG} is proved as described above and so on.

The iteration is continued until the difference between the modeled P, reflecting the *same* atmospheric conditions but *different* values of C_{FG} at each iteration step, and P calculated from the uncorrected SSM/I brightness temperatures is < 0.001. This is usually achieved within the first 10 iterations. Data gaps caused by masking out areas with a large L value are filled using temporal linear interpolation of C obtained for the day before and after the considered one. The accuracy of C would be close to 1% if determined only by the difference threshold used for the minimization, but the coarser spatial resolution of the involved atmospheric data and the variability of the sea-ice tie points due to varying sea-ice and snow properties limit the accuracy to about 10%.
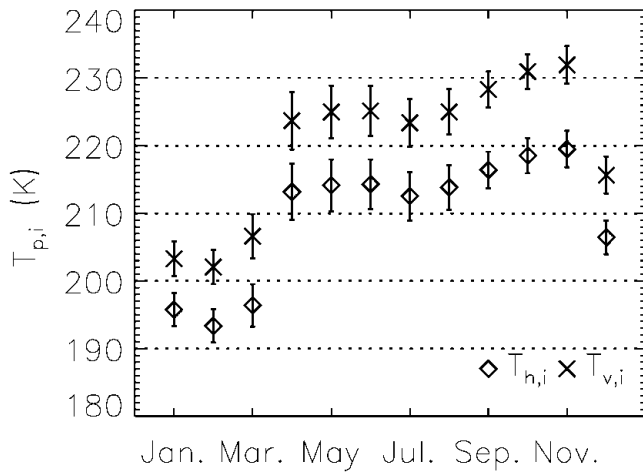
Fig. 2. Monthly 85 GHz sea-ice tie points T_{vi} and T_{hi} averaged over the period 1992–98. The error bars denote one standard deviation. Subscripts v and h refer to vertical and horizontal polarization, respectively.

3. RESULTS

Figures 2 and 3 show monthly 85 GHz sea-ice tie points averaged over the years 1992–98. Clearly, T_{vi} and T_{hi} are highly variable throughout the year. Freeze-up coincides well with a sharp increase of T_{vi} and T_{hi} in March/April (Fig. 2). The onset of melt is marked by a decrease of T_{vi} and T_{hi} from November to January. Remarkable are the low values of T_{hi} of about 200 K in summer. This corresponds to a surface emissivity of about 0.7 and may be caused by old refrozen coarse-grained snow. The gradual increase of T_{vi} and T_{hi} between August and November is probably a result of a growing liquid-water fraction in the snow, which increases the emissivities at both polarizations (Garrity, 1992). Values of P_i vary between 0.021 (January) and 0.028 (October) and are fairly constant within one standard deviation, which has been calculated from the standard deviations of T_{vi} and T_{hi}. Based on these sea-ice tie points, the SEA LION algorithm has been used to calculate daily Antarctic sea-ice concentrations C_{85} for 1992–98 from NSIDC daily gridded brightness temperatures. Hereafter, NASA Team sea-ice concentrations obtained with the extended weather correction (Heygster and others, 1996) are denoted
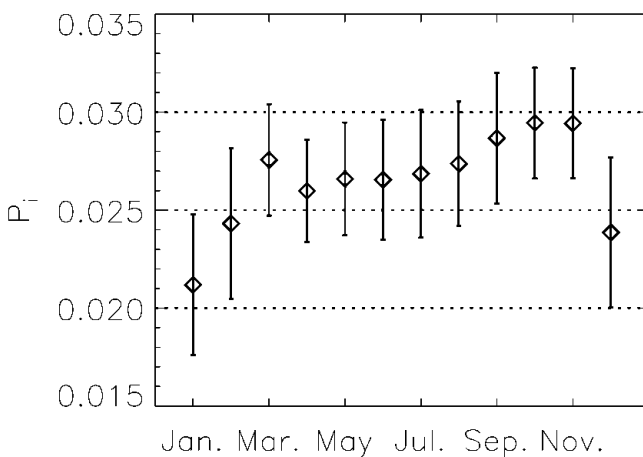

Fig. 3. Monthly 85 GHz sea-ice tie point P_i averaged over the period 1992–98. The error bars denote one standard deviation.
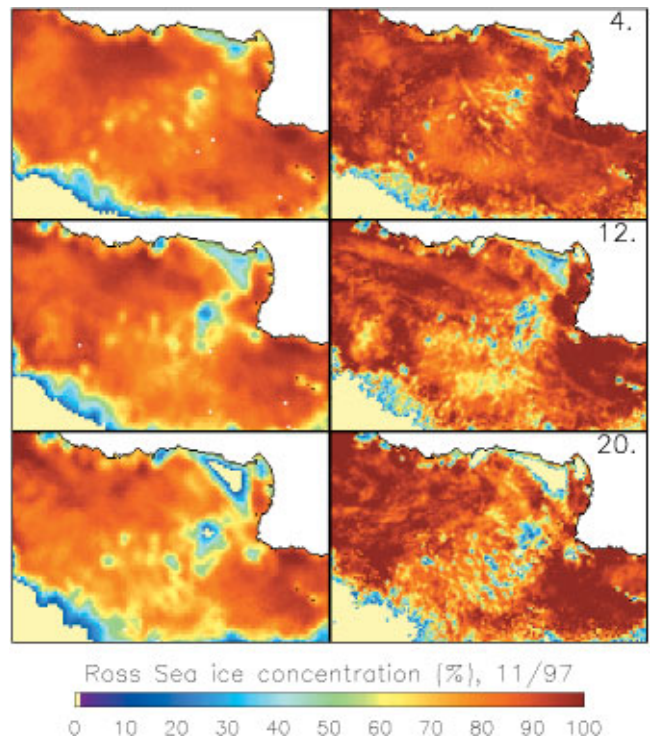

Ross Sea ice concentration (%), 11/97

Fig. 4. Evolution of the sea-ice cover in the Ross Sea, November 1997. Left panels: C_{NT}; right panels: C_{85}. Sea-ice concentrations <15% have been set to zero.

by C_{NT}, and Bootstrap sea-ice concentrations determined with seasonal coefficients by C_{BO}.

Figure 4 shows the beginning of the annual sea-ice decay in the Ross Sea in November 1997. More details can be identified in the images on the right side showing C_{85} than in those on the left showing C_{NT}. Figure 5 shows Operational Line-scan System (OLS) visible images of the Ross/Amundsen Sea region overlaid by the 15%, 60% and 90% isolines of C_{85} (Fig. 5a) and C_{NT} (Fig. 5b), on 16 November 1996. About 16 original OLS pixels have been averaged for one OLS pixel ($10 \times 10 \, km^2$) shown here. The isolines are mapped onto the NSIDC $12.5 \times 12.5 \, km^2$ grid. Several coastal polynyas and a decaying sea-ice cover typical for spring can be identified. The 15% isoline of C_{NT} appears only in one polynya (Fig. 5b) whereas C_{85} is <15% in almost every polynya (Fig. 5a). This seems to be quite reasonable since, during November, solar radiation accompanied by rising air temperatures stops the sea-ice production in coastal polynyas and keeps them open (Markus and others, 1998). First polynyas within the decaying pack ice (e.g. in the upper left (Amundsen Sea) and the lower right quarter (Ross Sea)) can be identified quite well by the 60% and sometimes even the 15% isoline of C_{85} (Fig. 5a). However, there is almost no correspondence between these areas and the 60% isoline of C_{NT} (Fig. 5b).

Sea-ice concentrations derived from in situ observations from the bridge of the research vessel *Nathaniel B. Palmer* in 1994–98 (C_{SHIP}) are compared to SSM/I sea-ice concentrations C_{SSMI}, which have been mapped onto the NSIDC $25 \times 25 \, km^2$ grid and rounded to the nearest tenth. Linear correlation coefficients for C_{SSMI} and C_{SHIP} lie between 0.528 (C_{85}) and 0.576 (C_{BO}). Average differences $C_{SSMI} - C_{SHIP}$ amount to -5% (C_{BO}), -10% (C_{85}) and -18% (C_{NT}). The most convincing linear regression is obtained with C_{85}: $C_{85} = 17.0 + 0.7 \times C_{SHIP}$.
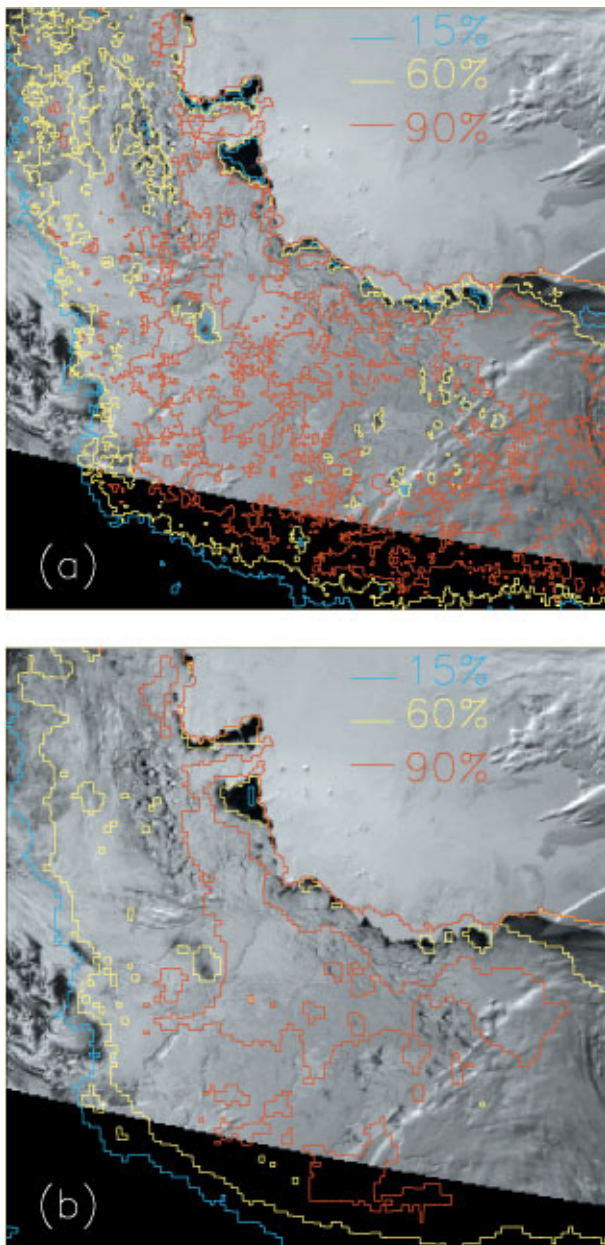
Fig. 5. OLS visible images overlaid with SSM/I sea-ice concentration isolines of 16 November 1996: (a) C_{85}, and (b) C_{NT}. The South Pole is at the upper right corner, and the right (top) image borders are along 180° W (90° W).

Daily sea-ice areas and extents are calculated from C_{SSMI} for 1992–98 (not shown). The annual and interannual variability of SEA LION sea-ice areas and extents shows reasonable agreement with those obtained from C_{BO} and C_{NT}, but for the SEA LION study period sea-ice extents and areas fall below those obtained from C_{BO}. The extent difference is 0.5×10^6 to $1.5 \times 10^6 \, \text{km}^2$. The areal difference is up to $0.5 \times 10^6 \, \text{km}^2$ in summer and 0.5×10^6 to $1.5 \times 10^6 \, \text{km}^2$ in winter. SEA LION sea-ice extents also fall below NASA Team sea-ice extents (by $10^6 \, \text{km}^2$ in summer and $0.5 \times 10^6 \, \text{km}^2$ in winter). SEA LION sea-ice areas are similar to NASA Team sea-ice areas in summer but exceed the latter by 0.5×10^6 to $1.5 \times 10^6 \, \text{km}^2$ in winter.

4. DISCUSSION AND CONCLUSIONS

The SEA LION algorithm uses the SSM/I 85 GHz polariza-tion together with monthly sea-ice and open-water tie points, and a weather correction scheme which is based on radiative transfer modeling. It provides daily Antarctic sea-ice concentration data with a spatial resolution of $12.5 \times 12.5 \, \text{km}^2$. Daily sea-ice extents and areas obtained from sea-ice concentration data obtained with the NASA Team (C_{NT}), the Bootstrap (C_{BO}) and the SEA LION (C_{85}) algorithm show reasonable agreement concerning the annual and inter-annual variability. However, in the regions studied, SEA LION generally provides a smaller sea-ice extent (by about $10^6 \, \text{km}^2$) throughout the year. The SEA LION sea-ice areas are similar to those obtained from sea-ice concentrations computed with the NASA Team and Bootstrap algorithms in summer but lie between them in winter.

A comparison of OLS visible images with coincident iso-lines of C_{85} and C_{NT} shows convincing results using SEA LION, particularly concerning the areal coverage by polynyas. Sea-ice concentration gradients provided by SEA LION are better resolved than those derived from the NASA Team algorithm. This may explain why the NASA Team or Bootstrap sea-ice extents are larger than the SEA LION sea-ice extent (more open-water pixels within the pack ice), while the NASA Team and Bootstrap sea-ice areas remain similar to the SEA LION sea-ice area (smaller net amount of sea-ice covered pixels, but higher average sea-ice concentration). We have also compared C_{85} with 850 ship observations of the sea-ice concentration for 1994–98. The results agree with those obtained with the NASA Team and Bootstrap algorithms.

The quality of the NWP model data, which are used for the correction of the atmospheric effect, and in particular of the cloud liquid-water content L, has a large impact on the retrieval of C_{85} and may cause significant errors. Further improvements of the atmospheric input parameters are necessary. Monthly sea-ice tie points seem to account for the annual evolution of the microwave signal of almost the entire Antarctic sea-ice cover, but smooth out regional variations. Dividing the ice pack into zones depending on the state of snow metamorphism, and estimating regional sea-ice tie points may be one step towards accounting for these vari-ations. This area requires further research, especially in the light of Figure 2 and when considering the findings of Drink-water (1998) concerning the seasonal backscatter variability of Antarctic sea ice.

The upcoming Advanced Microwave Scanning Radi-ometer (AMSR) on board the Adeos II and EOS Terra satel-lites operates at frequencies close to those of the SSM/I and is additionally equipped with 6 GHz channels. Due to technolo-gical advances, its data will allow an improvement of current sea-ice concentration products, mainly due to the enhanced spatial resolution of about $10 \times 10 \, \text{km}^2$, and probably in a more economical way than the method presented here, since a simple weather correction seems to be sufficient. The AMSR will provide 89 GHz data with a higher spatial resolution than the low AMSR frequencies. These data can be used to derive higher-resolved and thus more realistic sea-ice concentrations, at least under clear-sky conditions.

REFERENCES

Cavalieri, D. J. *and 6 others*. 1991. Aircraft active and passive microwave validation of sea ice concentration from the Defense Meteorological Satellite program special sensor microwave imager. *J. Geophys. Res.*, **96**(C12), 21,989–22,008.

Comiso, J. C., T. C. Grenfell, M. Lange, A.W. Lohanick, R. K. Moore and P. Wadhams. 1992. Microwave remote sensing of the Southern Ocean ice cover. Passive microwave signatures of sea ice. *In* Carsey, F. D. *and 7 others*, eds. *Microwave remote sensing of sea ice*. Washington, DC, American Geophysical Union, 243–259. (Geophysical Monograph Series 68.)

Drinkwater, M. R. 1998. Active microwave remote sensing observations of Weddell Sea ice. *In* Jeffries, M. O., *ed. Antarctic sea ice: physical processes, interactions and variability*. Washington, DC, American Geophysical Union, 187–212. (Antarctic Research Series 74.)

Fuhrhop, R. *and 6 others*. 1998. A combined radiative transfer model for sea ice, open ocean, and atmosphere. *Radio Sci.*, **33**(2), 303–316.

Garrity, K. 1992. Characterization of snow on floating ice and case studies of brightness temperature change during the onset of melt. *In* Carsey, F. D. *and 7 others*, eds. *Microwave remote sensing of sea ice*. Washington, DC, American Geophysical Union, 313–328. (Geophysical Monograph Series 68.)

Grenfell, T. C., J. C. Comiso, M. A. Lange, H. Eicken and M. R. Wensnahan. 1994. Passive microwave observations of the Weddell Sea during austral winter and early spring. *J. Geophys. Res.*, **99**(C5), 9995–10,010.

Grenfell, T. C. *and 11 others*. 1998. Evolution of electromagnetic signatures of sea ice from initial formation to the establishment of thick first-year ice. *IEEE Trans. Geosci. Remote Sensing*, **GE-36**(5), 1642–1654.

Heygster, G. *and 12 others*. 1996. *PELICON — Project for Estimation of Long-term variability in Ice CONcentration. Final report*. Bremen, University of Bremen. European Communities Environment Programme. (Contract EV5V-CT93-0268.)

Hollinger, J. P., R. Lo and G. Poe. 1987. *Special sensor microwave/imager user's guide*. Washington, DC, U.S. Naval Research Laboratory.

Karstens, U., C. Simmer and E. Ruprecht. 1994. Remote sensing of cloud liquid water. *Meteorol. Atmos. Phys.*, **54**, 157–171.

King, J. C. and J. Turner. 1997. *Antarctic meteorology and climatology*. Cambridge, Cambridge University Press.

Lomax, A. S., D. Lubin and R. H. Whritner. 1995. The potential for interpreting total and multiyear-ice concentrations in SSM/I 85.5 GHz imagery. *Remote Sensing Environ.*, **54**(1), 13–26.

Lubin, D., C. Garrity, R. O. Ramseier and R. H. Whritner. 1997. Total sea ice concentration retrieval from the SSM/I 85.5 GHz channels during the Arctic summer. *Remote Sensing Environ.*, **62**(1), 63–76.

Markus, T., C. Kottmeier and E. Fahrbach. 1998. Ice formation in coastal polynyas in the Weddell Sea and their impact on oceanic salinity. *In* Jeffries, M. O., *ed. Antarctic sea ice: physical processes, interactions and variability*. Washington, DC, American Geophysical Union, 273–292. (Antarctic Research Series 74.)

Massom, R. A., V. I. Lytle, A. P. Worby and I. Allison. 1998. Winter snow cover variability on East Antarctic sea ice. *J. Geophys. Res.*, **103**(C11), 24,837–24,855.

Maykut, G. A. 1978. Energy exchange over young sea ice in the central Arctic. *J. Geophys. Res.*, **83**(C7), 3646–3658.

Miao, J., K.-P. Johnsen, S. Kern, G. Heygster and K. Kunzi. 2000. Signature of clouds over Antarctic sea ice detected by the Special Sensor Microwave/Imager (SSM/I). *IEEE Trans. Geosci. Remote Sensing*, **GE-38**(5), 2333–2345.

Sturm, M., K. Morris and R. Massom. 1998. The winter snow cover of the West Antarctic pack ice: its spatial and temporal variability. *In* Jeffries, M. O., *ed. Antarctic sea ice: physical processes, interactions and variability*. Washington, DC, American Geophysical Union, 1–18. (Antarctic Research Series 74.)

Svendsen, E., C. Mätzler and T. C. Grenfell. 1987. A model for retrieving total sea ice concentration from a spaceborne dual-polarized passive microwave instrument operating near 90 GHz. *Int. J. Remote Sensing*, **8**(10), 1479–1487.

Ulaby, F. T., R. K. Moore and A. K. Fung. 1981. *Microwave remote sensing, active and passive. Vol. 1. Fundamentals and radiometry*. Reading, MA, Addison-Wesley Publishing Co.